Three-cluster model for the α-accompanied fission of californium nuclei

K. Manimaran and M. Balasubramaniam*
Department of Physics, Bharathiar University, Coimbatore 641 046, India
(Received 16 July 2008; revised manuscript received 19 January 2009; published 19 February 2009)

A three-cluster model is proposed to explain the particle-accompanied binary fission of radioactive nuclei. The model is developed as an extension of the preformed cluster model of Gupta and collaborators. The advantage of this model is that, for a fixed third fragment, we can calculate the fragmentation potential minimized in charge coordinate. For our study we chose the various neutron-deficient to neutron-rich californium nuclei, whose analysis reveals that the closed-shell effect of any one of the fragments in ternary fragmentation presents itself as the most favorable configuration to be observed. As one goes from a neutron-deficient to a neutron-rich californium isotope, the role of the neutron closed shell associated with any one of the preferred fragments changes to that of the proton closed shell, and for very neutron rich isotopes of californium the presence of a double closed shell nucleus enhances the decay probability. The quadrupole deformation of the light fragment (A_2) associated with the preferred configuration in the symmetric mass region also has a transition from positive to negative deformation as one goes from neutron-deficient to neutron-rich californium isotopes. The calculated relative yields of different fragmentation channels are compared with the available experimental yields for ^{252}Cf.

DOI: 10.1103/PhysRevC.79.024610 PACS number(s): 21.60.Gx, 25.85.Ca, 24.10.−i, 27.90.+b

I. INTRODUCTION

Californium (Cf) nuclei offer interesting possibilities for both theoretical and experimental investigations of various spontaneous decay modes. Spontaneous binary and ternary fission reactions of ^{252}Cf have been recently studied quite extensively [1–14], with ^{4}He, ^{10}Be, and ^{14}C nuclei observed as ternary fission particles. Ramayya *et al.* [12] measured the yield (on the order of 4×10^{-4} per 100 fission events) to the first excited state of ^{10}Be in the ^{96}Sr-^{146}Ba split of ^{252}Cf. Recently, Kopatch *et al.* [13] observed ^{5}He, ^{7}He, and ^{8}Li* (in its excited state of 2.26 MeV) isotopes as short-lived, intermediate, light charged particles (LCPs) in the ternary fission of ^{252}Cf. In another experiment, isotopes of He, Be, B, and C LCPs emitted with kinetic energy of more than 9, 21, 26, and 32 MeV, respectively, from ternary fission of ^{252}Cf were observed by Ter-Akopian *et al.* [14]. Using the improved triple-γ coincidence and α plus double-γ coincidence data of ^{252}Cf Goodin *et al.* [15] analyzed the bimodal fission of ^{252}Cf wherein the binary channels Xe-Ru and Ba-Mo, as well as the Ba-α-Zr, Mo-α-Xe, and Te-α-Ru ternary channels, were observed. Earlier, Lestone had shown [16,17] that ternary fission temperatures can be extracted by using the statistical theory of particle evaporation from hot compound nuclei, getting $T = 1.24 \pm 0.10$ MeV from the yields of hydrogen, helium, lithium, and beryllium isotopes ejected *perpendicular* to the direction of the main fragments from ^{233,235}U($n_{\rm th}$, f),^{239,241}Pu($n_{\rm th}$, f), and ^{250,252}Cf spontaneous fission, in near agreement with the experimental $T = 1.13 \pm 0.24$ MeV from the yields of *polar* α particles from ^{233,235}U($n_{\rm th}$, f). Very recently, Pyatkov *et al.* [18] have reported from three independent experiments a new island of high yields of ^{252}Cf(sf) collinear cluster tripartition (CCT) in the fragment mass space. The true ternary spontaneous decay channel observed and reported as CCT from these experiments has masses close to the magic ^{132}Sn, ^{70}Ni, and ^{48}Ca isotopes with a probability of not less than 4×10^{-3} with respect to binary fission, which is larger than the known ternary fission accompanied by LCPs. Apart from binary and ternary fissions of ^{252}Cf, for the (binary) cluster decay of ^{252}Cf, only the experimental attempt of Ortlepp *et al.* [19] resulted in an upper limit on the branching ratio B $[=T_{1/2}(\alpha)/T_{1/2}(\text{cluster})] \leqslant 10^{-8}$ for ^{46}Ar or ^{48}Ca clusters. For the ^{249}Cf isotope, more recently, Ardisson *et al.* [20] first attempted an indirect experiment to interpret the existence of an unassigned γ line (of 1554.2 keV in energy) in the spontaneous fission spectrum, following the α decay of ^{249}Cf, as a possible signature of ^{50}Ca emission from ^{249}Cf and deduced a branching ratio B $= 4.9 \times 10^{-9}$ [or $T_{1/2}(^{50}\text{Ca}) = 2.2 \times 10^{18}$ s], which in a later direct experiment [21] is pushed downward (or upward) to B $\leqslant 1.5 \times 10^{-12}$ [or $T_{1/2}(^{50}\text{Ca}) \geqslant 7.4 \times 10^{21}$ s]. Theoretically, it has been predicted by one of us [22] that ^{249,252}Cf parents present themselves as novel cases of emitting a doubly magic cluster ^{48}Ca or its neighboring nuclei ^{46}Ar and ^{50}Ca. If observed, the importance of the shell effects of the lighter (cluster) product, in addition to that of the already observed heavier (daughter) product, will be shown for the first time. The calculations [22] show that ^{46}Ar or ^{48}Ca are in fact the most probable decay products of ^{249,252}Cf parents, but the estimated decay half-life times are far more than the available upper limits. In other words, the calculations suggest that, with the presently available experimental methods, it will be difficult, if not impossible, to observe heavy-ion emission from either of these parents. It may, however, be mentioned that the inclusion of the effects of deformation and neck formation between the decay products could lead to a favorable situation. Another interesting result of these calculations is that, next to α decay, the lighter clusters ^{10}Be and ^{14}C are also preformed most favorably as binary decay products, but then, owing to the penetrability factor, their decay half-life times are predicted to be very large for the present-day experimental facilities. Since these clusters

*m.balou@gmail.com

are already observed as ternary fission products, a cascade or sequential decay of the corresponding binary decay daughter products could not be ruled out. Alternatively, it is possible that these lighter clusters are first preformed as binary decay products and then penetrate a three-body barrier.

From the published theoretical investigations [5–7] of the ternary fission of ^{252}Cf, it is seen that the closed-shell effect of any one of the two heavier fragments may also play an important role in ternary fission. However, in these theoretical studies, the probable ternary configuration is generally chosen by some intelligent guess or from the Q-value systematics. The most probable configuration, for the various particle-accompanied fission studies, reveals that, of the two heavy fragments, at least one of the fragments associates itself with the closed shell and in some cases even the doubly closed-shell nucleus, such as ^{132}Sn ($Z = 50$, $N = 82$), is seen. Obviously, it would be of interest to see the role of closed shell(s) of any one of the heavy fragments in the complete isotopic chain of the Cf nucleus. From the experimental observation of ^{4}He-accompanied fission of ^{252}Cf, it is seen that the fragment combination ^{145}Ba + ^{103}Zr is found to have the largest yield, when compared with other observed fragment combinations. This means that the role of the spherical closed shell alone is not enough, and, perhaps, the role of the deformed closed shell should also be taken into account since Zr is a deformed closed-shell nucleus. In the present study, however, we do not include the deformation effects of the fragments.

The obvious difficulty involved in the theoretical studies of ternary fission is the complete minimization of the potential energy for the mass asymmetry (defined later) involved in this process. In the case of binary fission of a nucleus having mass number A the mass asymmetry involved has only $A/2$ combinations, which further can be minimized with respect to the charge asymmetry. In the present work, we have attempted to study the complete mass asymmetry involved, at least for the α-accompanied ternary fission of neutron-deficient to neutron-rich Cf nuclei. Apparently, such a theoretical study of the Cf nucleus is warranted both for the guidance of future experiments and for investigating the novel closed-shell effects involved in this process. In other words, in this paper, we are interested to study the isotopic effect of the parent nucleus Cf with $N = 140$ to 158 for ($A_3 = 4$)-accompanied ternary fission.

II. THE THREE-CLUSTER MODEL

The three-cluster model (TCM) developed here is an extension of the preformed cluster model (PCM) of Gupta and collaborators for ground-state decays in cluster radioactivity (CR) and related phenomena [23–27]. Thus, like PCM, TCM is also based on the dynamical or quantum mechanical fragmentation theory of cold fusion phenomenon in heavy-ion reactions and fission dynamics, including the prediction of CR [28–31]. This theory is worked out in terms of

(i) the collective coordinate of mass (and charge) asymmetry

$$\eta = (A_1 - A_2)/(A_1 + A_2) \ [\eta_Z = (Z_1 - Z_2)/(Z_1 + Z_2)],$$

where 1 and 2 stand, respectively, for heavy and light fragments, and the third fragment in TCM is denoted by 3 and is fixed (and hence only the mass asymmetry between 1 and 2 is considered), and

(ii) relative separation R (defined later), which in TCM characterizes, respectively, (a) the nucleon division (or nucleon exchange) between the outgoing fragments and (b) the sharing of the available Q value to the kinetic energies E_i of the three fragments (i.e., $Q = E_1 + E_2 + E_3$), with the Q value for three decay products defined as

$$Q = M - \sum_{i=1}^{3} m_i, \tag{1}$$

where M is the mass excess of the decaying nucleus and m_i is the mass excesses of the product nuclei, expressed in MeV.

By using a decoupled approximation to R and η motions, in TCM, the decay constant is defined as

$$\lambda = P_0 P \nu P_3, \tag{2}$$

where P_0, the preformation probability, refers to η motion and P, the penetrability, to R motion. One of the assumptions of the TCM is that the preformation probability of the third fragment $P_3 = 1$ (here, the third fragment is an α particle). The preformation probability P_0 of fragment 2 (equivalently, of fragment 1) can also be calculated by solving the stationary Schrödinger equation in the η coordinate, at a fixed R, for the use of (ternary) fragmentation potential between the three nuclei, defined as

$$V_{\rm tot} = \sum_{i=1}^{3} \sum_{j>i}^{3} (B_{ii} + V_{ij}). \tag{3}$$

Here B_{ii} are the binding energies of the three fragments in energy units, taken from Refs. [32,33], and

$$V_{ij} = V_{Cij} + V_{Nij}, \tag{4}$$

with $V_{Cij} = Z_i Z_j e^2 / R^s{}_{ij}$, the Coulomb interaction between the three nuclei, and V_{Nij}, the short-range Yukawa plus exponential nuclear attractive potential among the three fragments,

$$V_{Nij} = -4 \left(\frac{a}{r_0}\right)^2 \sqrt{a_{2i} a_{2j}} [g_i g_j (4 + \xi) - g_j f_i - g_i f_j] \times \frac{\exp(-\xi)}{\xi}, \tag{5}$$

where $\xi = R^s{}_{ij}/a$, and the functions g and f are

$$g_k = \zeta \cosh \zeta - \sinh \zeta \tag{6}$$

and

$$f_k = \zeta^2 \sinh \zeta, \tag{7}$$

where $\zeta = R_k/a$ with the radius of the nucleus being $R_k = r_0 A_k^{1/3}$. Here $a = 0.68$ is the diffusivity parameter and the asymmetry parameter is $a_{2k} = a_s(1 - \omega I^2)$ with $a_s = 21.13$ MeV, $\omega = 2.3$, and $I = \frac{N-Z}{A}$. The relative separation is

$$R^s_{ij} = R_{ij} + s_{ij}, \tag{8}$$

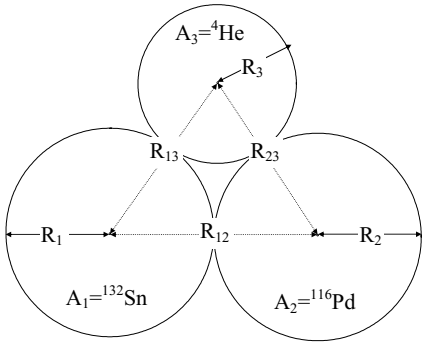

FIG. 1. A schematic touching configuration of three nuclei, with the parameters as labeled. The touching configuration is defined by the surface separation $s_{12} = s_{13} = s_{23} = 0$. The solid arrows define the radii of the fragments and the dotted arrow defines the center-to-center distance between the fragments.

with $R_{ij} = r_0(A_i^{1/3} + A_j^{1/3})$, where $r_0 = 1.44$ fm, the distance between the centers of any two nuclei. For the surface separation s_{ij},

$$s = s_{12} = s_{13} = s_{23} = 0 \tag{9}$$

corresponds to the touching configuration of the three fragments as shown in Fig. 1.

P_0 is the solution of the stationary Schrödinger equation in η, at a fixed $R = R_{ij}^s = R_{12} + s_{12}$ for the potential defined in Eq. (3) corresponding to the touching configuration ($s = 0$), as shown in Fig. 1,

$$\left[-\frac{\hbar^2}{2\sqrt{B_{\eta\eta}}}\frac{\partial}{\partial\eta}\frac{1}{\sqrt{B_{\eta\eta}}}\frac{\partial}{\partial\eta} + V_R(\eta)\right]\psi^\nu(\eta) = E^\nu\psi^\nu(\eta), \tag{10}$$

with $\nu = 0, 1, 2, 3, \ldots$ referring to ground-state ($\nu = 0$) and excited-state solutions. The solution is

$$P_0(A_i) = |\ \psi_R[\eta(A_i)]\ |^2\ \sqrt{B_{\eta\eta}}\frac{2}{A}, \tag{11}$$

where $i = 1$ or 2. The mass parameters $B_{\eta\eta}(\eta)$, representing the kinetic energy part in Eq. (10), are the smooth classical hydrodynamical masses [34]. In the decoupled approximation an equivalent Schrödinger equation for R motion can be used to find the probability $|\psi_\eta(R)|^2$. However, instead of solving the Schrödinger equation in R, the penetration probability is solved by using the WKB approximation as discussed in the following. It is to be mentioned here that, in this present work, the role of preformation probability is not studied. Rather, the relative yields for all the charge-minimized fragmentation channels are calculated as the ratio between the penetration probability of a given fragment over the sum of penetration probabilities of all possible fragmentation as

$$Y(A_i, Z_i) = \frac{P(A_i, Z_i)}{\sum P(A_i, Z_i)}. \tag{12}$$

The penetrability (i.e., the probability for which the ternary fragments to cross the three-body potential barrier) is the WKB integral,

$$P = \exp\left[-\frac{2}{\hbar}\int_{s_1}^{s_2}\{2\mu[V(s) - Q]\}^{1/2}ds\right], \tag{13}$$

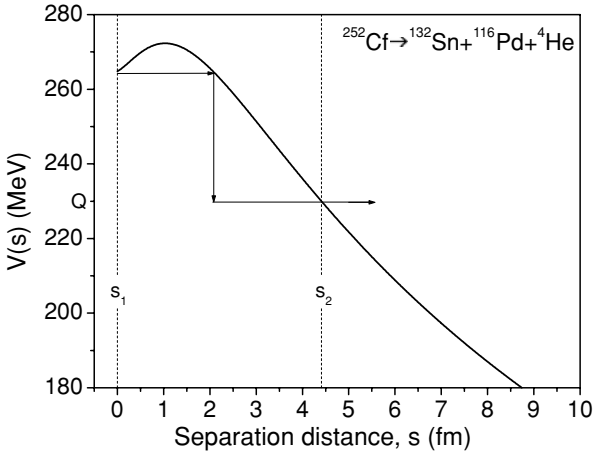

FIG. 2. The scattering potential as a function of the surface separation $s(= s_{12} = s_{13} = s_{23})$ of all three fragments. The decay path and the Q value are also labeled.

solved analytically [24], with $s_1 = 0$, the touching configuration, as the first turning point and s_2 as the second turning point (see Fig. 2) satisfying

$$V(s_2) = Q. \tag{14}$$

It is to be mentioned here that this action integral depends only on the variable s. The potential is calculated by varying the value of s uniformly among all three fragments as defined in Eq. (9). Fitting to the experimental data can be done if one considers a different variation of the separation distance s_{12} between fragments 1 and 2 as

$$s = k * s_{12} = s_{23} = s_{13}. \tag{15}$$

This parameter k assimilates the effects of deformation by lowering the barrier (i.e., as the value of k decreases the barrier will also decrease). An exact fitting to the experimental data can also be done by fine-tuning this parameter individually for each channel. The reduced mass of the three fragments is defined as

$$\mu_{123} = \left(\frac{\mu_{12}A_3}{\mu_{12} + A_3}\right)m, \tag{16}$$

where m is the nucleon mass and

$$\mu_{12} = \frac{A_1A_2}{A_1 + A_2}, \tag{17}$$

with $R_0 = r_0A^{1/3}$ as the radius of the spherical compound nucleus.

III. RESULTS AND DISCUSSION

First, the ternary fragmentation potential, as defined in Eq. (3), is calculated for ^{252}Cf as the representative parent nucleus with third-particle mass fixed as $A_3 = 4$. For the mass-four nucleus, one has three possible charge numbers, corresponding to ^{4}H, ^{4}He, and ^{4}Li, leaving the remaining system as ^{248}Bk, ^{248}Cm, and ^{248}Am, respectively, whose binary fragmentation ($A_1 + A_2$), minimized in charge asymmetry

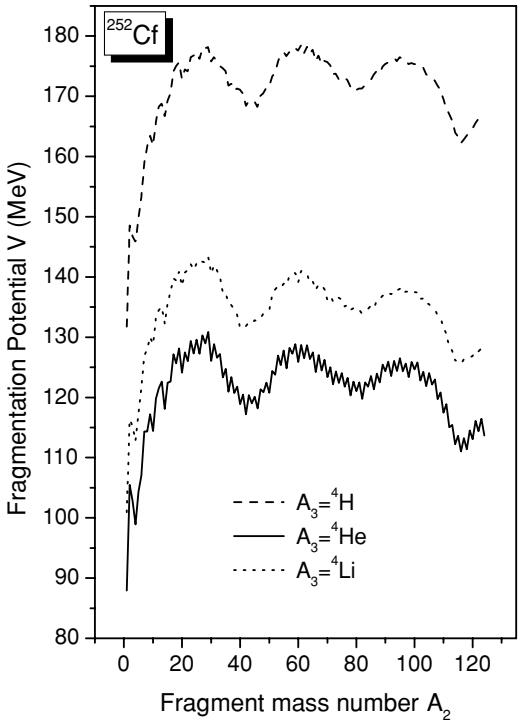

FIG. 3. The ternary fragmentation potential for ^{252}Cf nuclei for different $A_3 = 4$ combinations.

coordinate η_Z, is considered. The resulting ternary fragmentation potentials for the three possible fixed $A_3 = 4$ nuclei are presented in Fig. 3. It is interesting to see from this figure that the ternary fragmentation potential corresponding to $A_3 = {}^4$He lies lowest of all the three potentials. This means that the ternary fission of ^{252}Cf is most favored with the third particle as ^{4}He, shown here for the first time. In other words, in our calculations, the third particle is not chosen simply as ^{4}He; rather it is obtained in the energy minimization with respect to the charge of the A_3 fragment. The same result (i.e., ^{4}He as the third particle) is obtained for all the remaining parent nuclei, whose resulting ternary fragmentation potentials are presented in Fig. 4. The interesting result of this figure is that the deepest minima (marked for each parent nucleus) refer to the neutron closed shell $N = 82$ (for ^{138}Ba, ^{136}Xe, and ^{134}Te nuclei) for neutron-deficient parents $^{238-248}$Cf (upper panel) but to the proton closed shell $Z = 50$ (for ^{130,132}Sn nuclei) for neutron-rich parents $^{250-256}$Cf (lower panel). For $^{248-256}$Cf parents the regions of cold fragmentation exist in the three-body fragmentation potential. Among them the third one has the strong minimum corresponding to spherical Sn nuclei, similar to that of the cold binary fissions.

The important result is that, as we go from neutron-deficient to neutron-rich Cf isotope, the neutron closed shell associated with the heavier fragment (A_1, Z_1) of the preferred configuration in the cold valley changes to the proton closed shell associated with the heavier fragment of the preferred configuration and this becomes even doubly closed shell for very neutron rich $^{252-256}$Cf isotopes. It is to be mentioned here that in all the most probable configurations lying in the cold valley at symmetric mass region (as labeled in Fig. 4), the heavier fragment (A_1, Z_1) quadrupole deformation (β_2) is zero. But at the same time the associated light fragment (A_2, Z_2) has considerable quadrupole deformation, as shown in Fig. 5. The deformation values are taken from Ref. [33]. It is interesting to see in this figure that for the neutron-deficient $^{238-246}$Cf isotopes, the deformation of the light

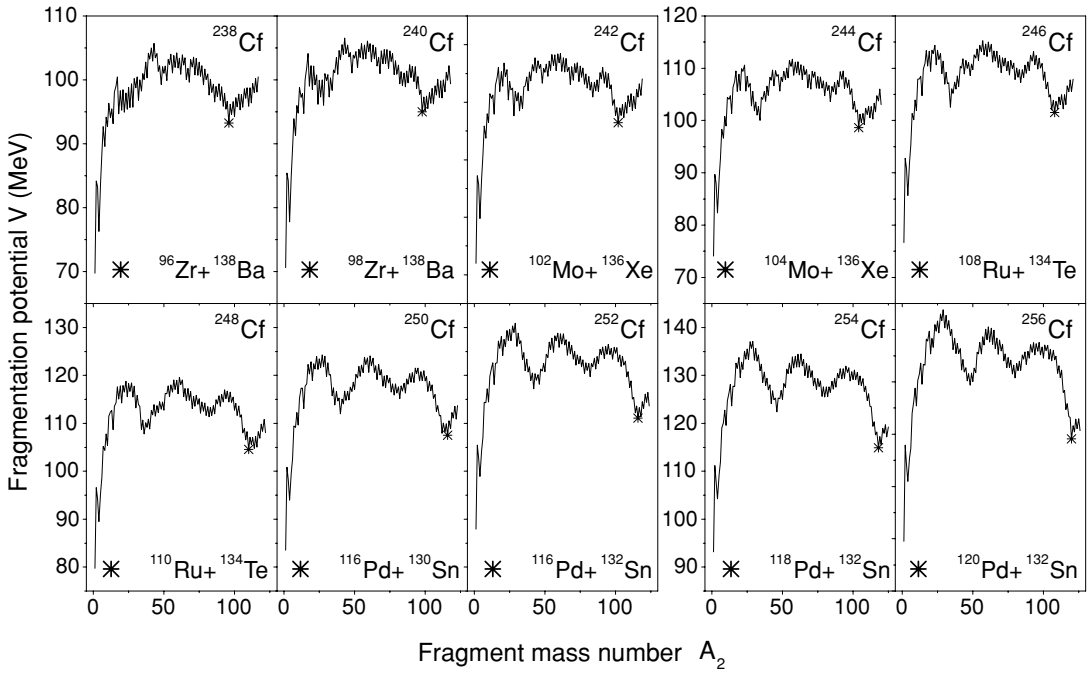

FIG. 4. The ternary fragmentation potential for $^{238-256}$Cf nuclei. The minimized third fragment (A_3) in all cases is ^{4}He. The most probable configurations $A_1 + A_2$ near the symmetric mass region are marked with $*$ symbols and are also labeled.

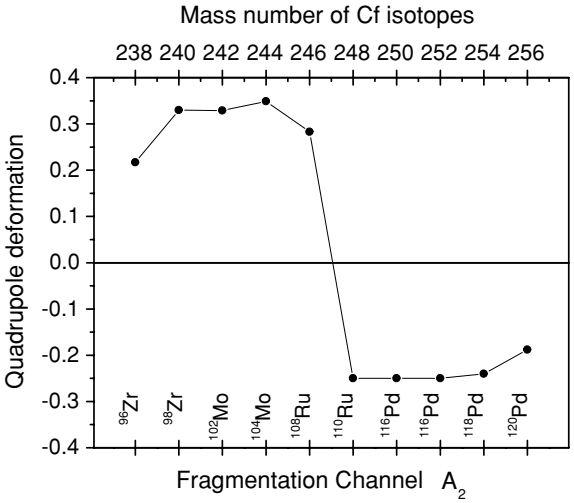

FIG. 5. The quadrupole deformation β_2 of the light fragment A_2 associated with the most probable configuration in the symmetric mass region for $^{238-256}$Cf nuclei.

fragment (A_2, Z_2) has positive quadrupole deformation, which changes to negative quadrupole deformation for the neutron-rich $^{248-256}$Cf isotopes. The transition of neutron closed shell to proton closed shell associated with the heavier fragment (A_1, Z_1) and a similar transition in the quadrupole deformation of the associated light fragment (A_2, Z_2) are seen as one goes from neutron-deficient to neutron-rich Cf. The deformation in the potential comes only through the binding energies.

In Fig. 6, we have plotted the results of our calculated relative yield [as defined in Eq. (12)] of the α-accompanied ternary fragmentation for all the considered isotopes of Cf nuclei. In this figure the y-axis scale in all the panels is the same and also the relative yields are shown as a function of fragment mass numbers A_2 and A_1 by taking their values between 75 to 175. For $A_2 < 75$ and $A_1 > 175$ the relative yields are nearly zero. A two-humped structure in the mass distribution is seen in all cases. For neutron-deficient Cf isotopes, a wider distribution is seen; this becomes distinct and narrower for neutron-rich Cf isotopes. Also, the magnitude of the relative yield corresponding to the preferred fragments as labeled increases with increasing neutron number of the parents. The minimum obtained in the fragmentation potential (as labeled in Fig. 4, near the symmetric mass region) is the same as for the most probable fragments in the relative yield calculations as well except for the cases of ^{240}Cf and ^{248}Cf. For ^{240}Cf the minimum in the potential corresponds to the configuration of ^{138}Ba + ^{98}Zr whereas the relative yield is maximum for the configuration of ^{136}Xe + ^{100}Mo because the Q value corresponding to the ^{136}Xe + ^{100}Mo configuration is 228.75 MeV and the Q value corresponding to ^{138}Ba + ^{98}Zr is 225.56 MeV. Because of the higher Q value the fragment combination ^{136}Xe + ^{100}Mo has the highest yield for the parent ^{240}Cf. Similarly, for ^{248}Cf the minimum in the potential corresponds to the configuration ^{134}Te + ^{110}Ru but the relative yield is numerically maximum for ^{130}Sn + ^{114}Pd and the value of the relative yield for the configuration corresponding to ^{134}Te + ^{110}Ru differs with ^{130}Sn + ^{114}Pd only in the second decimals. The close values of these two may be because the Q values differ slightly as 228.64 and 227.52 MeV for ^{130}Sn + ^{114}Pd and ^{134}Te + ^{110}Ru, respectively.

In Fig. 7 we present a comparison of our calculated results corresponding to various separation distances between

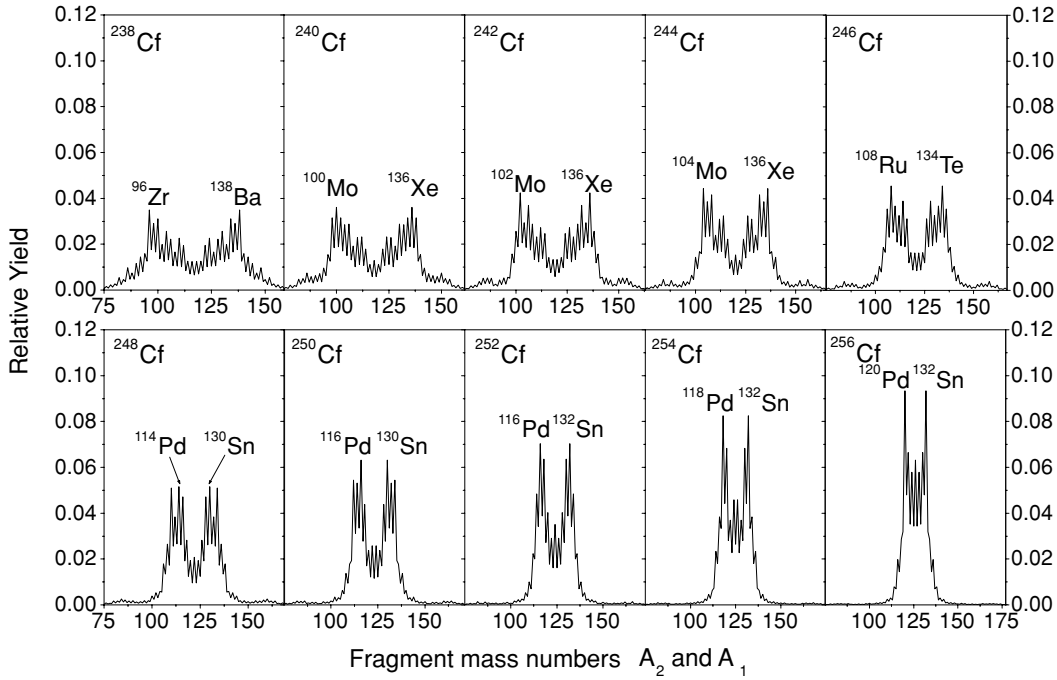

FIG. 6. The calculated relative yields for $^{238-256}$Cf nuclei. The minimized third fragment (A_3) in all cases is ^{4}He. The most probable configurations A_1 and A_2 are labeled. The scale of the y axis is the same in all panels.

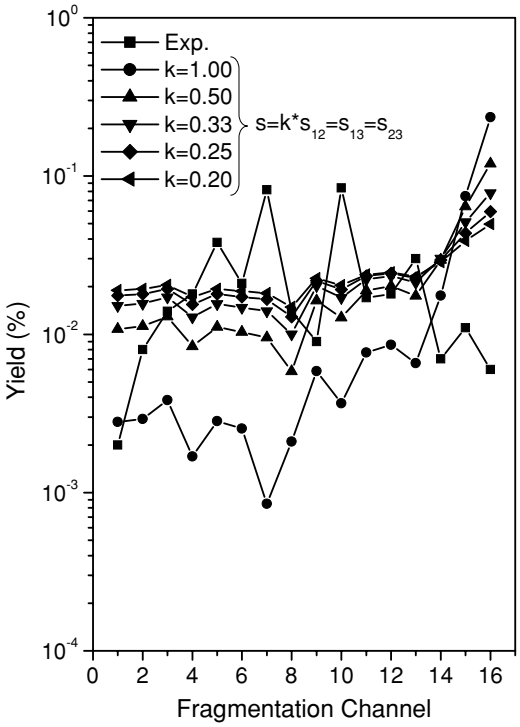

FIG. 7. The relative yields calculated at different separation distance between fragments 1 and 2 as defined by the parameter k in Eq. (15), compared with the experimental percentage yields for different fragmentation channels of the ^{252}Cf nucleus.

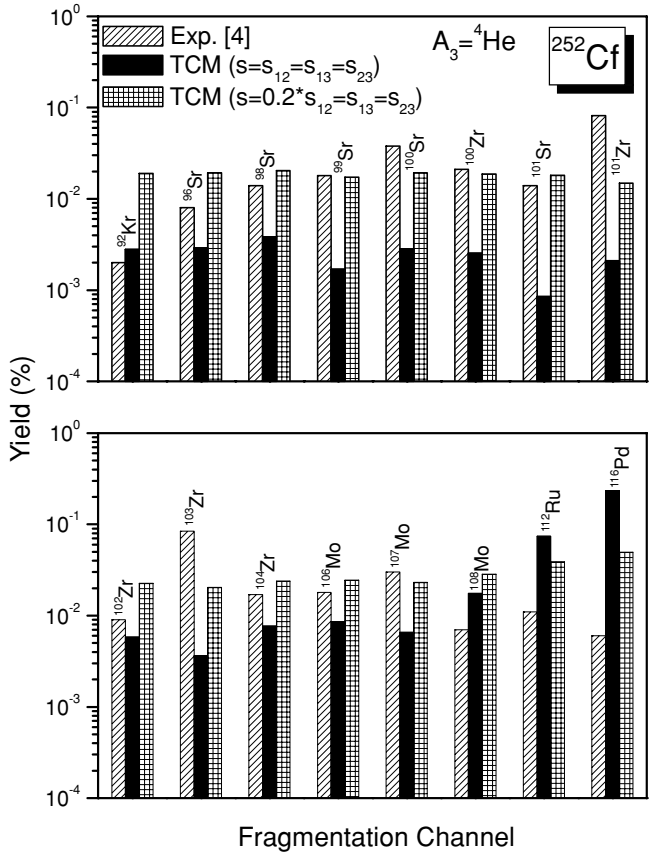

FIG. 8. Same as Fig. 7, but presented here as histograms for better comparison for the values of $k = 1$ and 0.2.

fragments 1 and 2 as defined in Eq. (15) for different values of k. The solid squares connected by lines correspond to the experimental data. The solid circles correspond to the case of $k = 1$. As the k value decreases (and hence the separation distance between fragments 1 and 2 increases) the strong oscillatory structure present in the calculations corresponding to $k = 1$ vanishes and becomes nearly a constant value for the lowest k value considered ($k = 0.2$). The calculated yields increase with the decrease in the value of the parameter k. In Fig. 8, for better comparison, our calculated yields for two different values of the parameter k (normalized to the total experimental yield) are compared with the measured percentage yields for the ^{252}Cf nucleus. In this figure, the hatched histograms are the measured yields and the black ones are the calculated relative normalized yields for $k = 1$ (corresponding to uniform separation of the three fragments) and the checked histograms correspond to $k = 0.2$. Obviously, it is seen in this figure clearly that the lowering of the barrier by the introduction of the parameter k increases the yield, which is in good agreement with that of the experimental data. This parameter can further be fine-tuned to get an exact fitting for each channel though this is not attempted here. In all cases the third particle is ^{4}He. The lighter fission fragments (A_2, Z_2) are labeled above the corresponding histograms. The calculated relative yields are for the charge minimized fragmentation channels. In other words, these channels are revealing themselves during the minimization of the fragmentation potential, except for $A_2 = 101$. For $A_2 = 101$, in our calculations, the minimized configuration corresponds to the element Y with charge number $Z_2 = 39$. From the experimental data of these yields taken from Ref. [4], for mass numbers $A_2 = 100$ and 101, the relative percentage yields were measured for two charges (Sr and Zr with $Z_2 = 38$ and 40). Since, in the present model, we never exclude any possible fragmentations, we have presented the results for ^{100}Zr, ^{101}Sr, and ^{101}Zr. Though the actual minimum obtained for the mass number $A_2 = 100$ is ^{100}Sr, we have presented the result of ^{100}Zr as well. Similarly, though the actual minimum obtained for the mass number $A_2 = 101$ is ^{101}Y in our calculations, we have presented our results of ^{101}Sr and ^{101}Zr as well in this figure.

The two different charge dispersions corresponding to these two mass numbers $A_2 = 100$ and 101 can be explained by our calculations as presented in Fig. 9. This figure presents the charge dispersion potential $V(\eta_z)$ and Q values for $A_2 = 100$ and 101 as a function of different fragment charge number Z_2. It is very clearly seen from this figure that, for the fragmentation potential of $A_2 = 100$, the potential energy values corresponding to Sr and Zr are equally competing, though numerically Sr has a potential energy value lower than that of Zr. But, at the same time, Zr becomes a possible charge combination for this mass number because of its higher Q value as presented in this figure. Similarly, for the odd mass number $A_2 = 101$, the fragmentation potential $V(\eta_z)$ shows indistinguishable minima between Y and Zr, but numerically Y has the minimum value, but again Zr becomes a possible

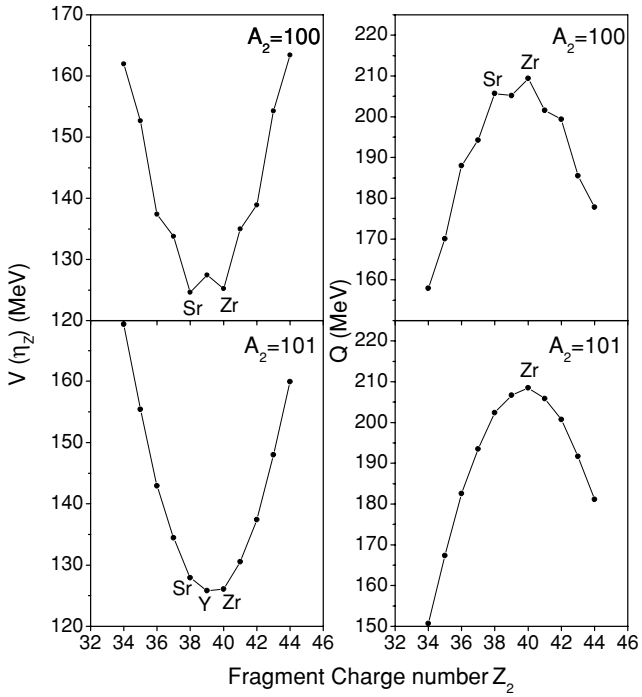

FIG. 9. The fragmentation potentials and the Q values for the fragment mass numbers $A_2 = 100$ and 101 as a function of charge numbers Z_2.

candidate because of its higher Q value as presented in this figure.

In all the cases compared in Fig. 8, our calculated results corresponding to the parameter $k = 1$ are underestimating the experimental yields, except for the last three channels. This has been overcome by the introduction of the parameter k. For the lowest k value considered in our calculations our results are in good agreement with the measured yields. The parameter k may be playing the role of deformation. It is known that the inclusion of deformation in the interaction potential will considerably lower the barrier. Hence its implication in the results needs to be studied and may favor a better agreement between the calculated values and the experimental values.

IV. SUMMARY

A three-cluster model is developed for explaining ternary fission of heavy radioactive nuclei. The model is applied to study neutron-deficient to neutron-rich Cf nuclei. The charge minimization of the third fragment is shown here for the first time. Moreover, the most favorable combination is also being revealed as a result of studying the complete mass asymmetry of the system by minimizing the potential energy rather than by making a mere guess. The importance of the closed shell and the deformation associated with the most favorable configuration are emphasized. For the most favorable ternary configurations the role of the neutron closed shell plays a crucial role in neutron-deficient parent nuclei and a transition from neutron closed shell to proton closed shell takes place as the neutron number of the parent nuclei increases. For very neutron rich nuclei it is seen that the role of a doubly magic closed shell seems to become important. Our calculated relative percentage yields are in reasonable agreement with the experimental values.

ACKNOWLEDGMENT

One of the authors K.M. acknowledges with thanks the financial support of Bharathiar University by granting him a university research Grant No. C2/URF/PHYS/2007.

[1] F. Gönnenwein, A. Möller, M. Cröni, M. Hesse, M. Wöstheinrich, H. Faust, G. Fioni, and S. Oberstedt, Nuovo Cimento A **110**, 1089 (1997).

[2] A. Möller, M. Cröni, F. Gönnenwein, and G. Petrov, in *Proceedings International Conference on Large Amplitude Motion in Nuclei, Brolo, Italy, 1996*, edited by C. Giardina (World Scientific, Singapore, 1996), p. 203.

[3] A. Săndulescu, A. Florescu, F. Carstoiu, and W. Greiner, J. Phys. G: Nucl. Part. Phys. **23**, L7 (1997).

[4] A. V. Ramayya, J. H. Hamilton, J. K. Hwang, L. K. Peker, J. Kormicki, B. R. S. Babu, T. N. Ginter, A. Săndulescu, A. Florescu, F. Carstoiu, W. Greiner, G. M. Ter-Akopian, Yu. Ts. Oganessian, A. V. Daniel, W. C. Ma, P. G. Varmette, J. O. Rasmussen, S. J. Asztalos, S. Y. Chu, K. E. Gregorich, A. O. Macchiavelli, R. W. Macleod, J. D. Cole, R. Aryaeinejad, K. Butler-Moore, M. W. Drigert, M. A. Stoyer, L. A. Bernstein, R. W. Lougheed, K. J. Moody, S. G. Prussin, S. J. Zhu, H. C. Griffin, and R. Donangelo, Nuovo Cimento A **110**, 1073 (1997); Phys. Rev. C **57**, 2370 (1998).

[5] A. Săndulescu, A. Florescu, F. Carstoiu, A. V. Ramayya, J. H. Hamilton, J. K. Hwang, B. R. S. Babu, and W. Greiner, Nuovo Cimento A **110**, 1079 (1997).

[6] A. Săndulescu, F. Carstoiu, I. Bulboaca, and W. Greiner, Phys. Rev. C **60**, 044613 (1999).

[7] D. N. Poenaru, W. Greiner, J. H. Hamilton, A. V. Ramayya, E. Hourany, and R. A. Gherghescu, Phys. Rev. C **59**, 3457 (1999).

[8] A. Florescu, A. Săndulescu, D. S. Delion, J. H. Hamilton, A. V. Ramayya, and W. Greiner, Phys. Rev. C **61**, 051602(R) (2000).

[9] F. Carstoiu, I. Bulboaca, A. Săndulescu, and W. Greiner, Phys. Rev. C **61**, 044606 (2000).

[10] S. Misicu, P. O. Hess, and W. Greiner, Phys. Rev. C **63**, 054308 (2001).

[11] D. S. Delion, A. Florescu, and A. Săndulescu, Phys. Rev. C **63**, 044312 (2001).

[12] A. V. Ramayya, J. K. Hwang, J. H. Hamilton, A. Sandulescu, A. Florescu, G. M. Ter-Akopian, A. V. Daniel, Yu. Ts. Oganessian, G. S. Popeko, W. Greiner, and J. D. Cole (GANDS95 Collaboration), Phys. Rev. Lett. **81**, 947 (1998).

[13] Yu. N. Kopatch, M. Mutterer, D. Schwalm, P. Thirolf, and F. Gonnenwein, Phys. Rev. C **65**, 044614 (2002).

[14] G. M. Ter-Akopian, A. V. Daniel, A. S. Fomichev, G. S. Popeko, A. M. Rodin, Yu. Ts. Oganessian, J. H. Hamilton, A. V. Ramayya, J. Kormicki, J. K. Hwang, D. Fong, P. Gore,

J. D. Kole, M. Jandel, J. Kliman, L. Krupa, J. O. Rasmussen, I. Y. Lee, A. O. Macchiavelli, P. Fallon, M. A. Stoyer, R. Donangelo, S. C. Wu, and W. Greiner, Phys. At. Nucl. **67**, 1860 (2004).

[15] C. T. Goodin, D. Fong, J. K. Hwang, A. V. Ramayya, J. H. Hamilton, K. Li, Y. X. Luo, J. O. Rasmussen, S. C. Wu, M. A. Stoyer, T. N. Ginter, S. J. Zhu, R. Donangelo, G. M. Ter-Akopian, A. V. Daniel, G. S. Popeko, A. M. Rodin, and A. S. Fomichev, Phys. Rev. C **74**, 017309 (2006).

[16] J. P. Lestone, Phys. Rev. C **70**, 021601(R) (2004).

[17] J. P. Lestone, Phys. Rev. C **72**, 014604 (2005).

[18] Yu. V. Pyatkov, D. V. Kamanin, W. H. Trzaska, W. Von Oertzen, S. R. Yamaletdinov, A. N. Tjukavkin, V. G. Tishchenko, V. G. Lyapin, Yu. E. Peinionzhkevich, A. A. Alexandrov, and S. V. Khlebnikov, Roman Rep. Phys. **59**, 569 (2007).

[19] H.-G. Ortlepp, R. Kotte, and F. Stary, in *Proceedings 15th International Symposium on Nuclear Physics, Nuclear Fission, Gaussing, East Germany*, edited by D. Seelinger *et al*., 11–15 November 1985, p. 35.

[20] G. Ardisson, A. A. Koua, and G. Barci-Funel, J. Radiol. Nucl. Chem. **227**, 177 (1998).

[21] G. Ardisson, V. Barci, J. F. Le Du, D. Trubert, R. Bonetti, A. Guglielmetti, and R. K. Gupta, Phys. Rev. C **60**, 037301 (1999).

[22] M. Balasubramaniam and R. K. Gupta, Phys. Rev. C **60**, 064316 (1999).

[23] R. K. Gupta, in *Proceedings of the 5th International Conference on Nuclear Reaction Mechanisms, Varenna, 1988*, edited by E. Gadioli (Ricerca Scientifica ed Educazione Permanente, Milano, 1988), p. 416.

[24] S. S. Malik and R. K. Gupta, Phys. Rev. C **39**, 1992 (1989).

[25] R. K. Gupta, W. Scheid, and W. Greiner, J. Phys. G: Nucl. Part. Phys. **17**, 1731 (1991).

[26] S. Kumar and R. K. Gupta, Phys. Rev. C **49**, 1922 (1994).

[27] R. K. Gupta, in *Heavy Elements and Related New Phenomena*, edited by W. Greiner and R. K. Gupta (World Scientific, Singapore, 1999), Vol. II, p. 730.

[28] R. K. Gupta, Sov. J. Part. Nucl. **8**, 289 (1977).

[29] J. A. Maruhn, W. Greiner, and W. Scheid, in *Heavy Ion Collisions*, edited by R. Bock (North Holland, Amsterdam, 1980), Vol. 2, Chapter 6.

[30] A. Săndulescu, D. N. Poenaru, and W. Greiner, Sov. J. Part. Nucl. **11**, 528 (1980).

[31] R. K. Gupta and W. Greiner, in *Heavy Elements and Related New Phenomena*, edited by W. Greiner and R. K. Gupta (World Scientific, Singapore, 1999), Vol. I, p. 536.

[32] G. Audi and A. H. Wapstra, Nucl. Phys. **A595**, 4 (1995).

[33] P. Möller, J. R. Nix, W. D. Myers, and W. J. Swiatecki, At. Data Nucl. Data Tables **59**, 185 (1995).

[34] H. Kröger and W. Scheid, J. Phys. G **6**, L85 (1980).